To appear in the Journal of the Mechanics and Physics of Solids

Shock Attenuation Characteristics of Methylcellulose Hydrogels: Phenomenological Modeling

Orel Guetta, Bat Hen Varfman, Daniel Rittel*

Faculty of Mechanical Engineering, Technion – Israel Institute of Technology, 3200008 Haifa, Israel

Abstract

The shock attenuation characteristics of aqueous methylcellulose (MC) gels were characterized experimentally and modelled towards their application in bodily protection systems against traumatic injury. The attenuation of MC gel with 4 different thicknesses (4, 7, 10 and 20mm) and 3 concentrations (5, 10 and 15%Wt) was measured, using an instrumented (Hopkinson) bar and piezoresistive sensors for direct force sensing on the gel. First, the impulse attenuation was systematically characterized for all combinations of thickness and composition, and the results were analyzed statistically. The impulse attenuation increases with both thickness and MC concentration. A non-linear function was then fitted to the experimental results. The fitted functions increase monotonically with both the thickness and the concentration of the gel layer. However, the slope of each function decreases gradually with the thickness of the layer, thereby indicating an effective thickness beyond which shock attenuation efficiency does not increase significantly.The frequency dependence of the attenuation was determined next and found to be relatively independent of both thickness and gel concentration up to 100 kHz. A phenomenological expression was developed and validated for the shock attenuation of MC gels as a function of their composition, thickness and spectral content of the shock.

*Corresponding author

Email addresses: orel-gueta@campus.technion.ac.il (Orel Guetta), bathenv@campus.technion.ac.il (Bat Hen Varfman), merittel@technion.ac.il (Daniel Rittel)

Keywords: Aqueous methylcellulose, Thermoreversible gelation, Shock loading, Impulse mitigation

---

List of symbols

MC	methyl cellulose
SHPB	split Hopkinson pressure bar
SG	strain gauge
FF	FlexiForce$^{\text{TM}}$ sensors
T	thickness
C	concentration
f	frequency
t	time
MAD	median absolute deviation
ANOVA	analysis of variance
F_{in}	incoming force
F_{out}	outcoming force
$\tilde{H}(f)$	estimated frequency response function
$\tilde{S}_{xx}(f)$	power spectral density
$\tilde{S}_{xy}(f)$	cross power spectral density
J_{in}	incoming impulse
J_{out}	outcoming impulse
AF	impulse attenuation factor
μ	group mean
σ	standard deviation
$\alpha, \beta, \gamma, \delta$	frequency attenuation model constants
a, b	impulse model constants
$\varepsilon(T, C)$	impulse and spectral model coefficient
$\tilde{f}(f)$	force in frequency domain
$\mathcal{F}(z)$	Fourier transform
J^*_{out}	outcoming impulse before $\varepsilon(T, C)$ multiplication

1. Introduction

Methyl cellulose (MC) hydrogels are known to undergo thermo-reversible gelation (liquid to solid) upon heating. Unlike most materials, the solidification of MC gels is an endothermic process [1]. The energy for the gelation of MC can be supplied either by heating or, as recently observed, by mechanical impact [2]. When applying mechanical impact on MC, the shock can be absorbed by the endothermic gelation without involving any additional heat supply. High-speed imaging of the impact zone reveals that this transition occurs in a matter of a few microseconds, in the vicinity of impacted zone only, over an estimated thickness of *ca.* 5 mm [2]. Since the liquid phase of the solution is transparent and the solid phase is opaque, one can clearly see the solidification of the solution in the impact zone, as reported in [2].

Several recent reports have demonstrated an outstanding feature of MC gels in that they can significantly mitigate impact energy, thereby partially shielding engineering structures from the violent initial elastic accelerations inherent to shock loading [3]. Those accelerations are precisely the factor that is responsible for traumatic organ injury for instance [4],especially in the absence of noticeable damage or bodily penetration. In that aspect, MC gels are a newcomer to the family of shock shielding materials that have been extensively investigated, such as foams or rheological solutions [5]. In addition to their reported outstanding performance, MC gels are both cheap and present absolutely no health hazard, noting that they are also used as food additives [6].

Moreover, it appears that MC gels perform best for violent shocks with a short rise time [7] [8], pointing to the loading rate as opposed to the absolute load or impulse itself. This feature has been recently illustrated by Senol et al. [3] who compared the performance of MC gels using a shock tube and a Split Hopkinson bar. Their observation was that, although the absolute energy applied by the shock tube was greater than that of the Hopkinson bar, the latter applies this energy at a much greater loading rate, resulting in a noticeably higher impulse attenuation.

One of the widespread setups used to examine the dynamic properties of materials is the Split Hopkinson Pressure Bar (SHPB), also known as Kolsky apparatus [9] [10]. Briefly stated, the device consists two elastic slender bars, pressure tank and a striker. The bars are coaxial, have the same section area and free to move in the axial direction. The bars are usually instrumented with strain gauges (SG) at their mid-length. In our system we used conventional 12.7mm diameter SHPB apparatus, made of 7075-T6 aluminum-alloy bars and projectile. The impact of the gas-propelled striker generates a stress wave that is recorded by the strain gauges, as incident, reflected and transmitted pulses, respectively. Those pulses are then reduced into stresses and strains experienced by the specimen sandwiched between the two elastic bars.

However, soft polymers, such as Methyl Cellulose, have a low acoustic impedance, contrary to metals. This impedance mismatch between the metal bar/gel materials makes it difficult to test soft polymers in a common metallic SHPB setup [11]. Specifically, the transmitted wave's magnitude is nearly zero, and the incident wave is almost completely reflected backwards to the incident bar, which amounts basically to meeting a free-edge condition, as noted long ago by Kolsky about the testing of polymers [9].

To overcome this issue, it is possible to use thin piezoelectric or piezoresistive sensors to measure the applied forces directly [12] [13]. The piezoresistive sensors, such as those manufactured by FlexiForce^{TM} (FF) are 0.2mm thick with force sensing resolution of 0.1N, making them suitable for measuring small magnitude forces in dynamic tests for soft polymers without any interference in the experimental setup, as reported earlier by Richler and Rittel [13]. Note that this method renders the use of strain gauges unnecessary, except for the assessment of the incident pulse before it reaches the specimen.

The systematic characterization of shock impulse attenuation, as a function of the frequency content, MC gel layer thickness and composition is still missing, so that a constitutive equation for the attenuation has not been proposed yet. This is precisely the goal of the present paper, so that shock attenuating gels can be efficiently incorporated in the engineering design of shock protection systems.

2. Materials and Methods

2.1. Gel preparation

Methyl cellulose powder, according to the requested concentration - 5, 10 or 15%Wt - was weighed and added to water. The suspension was mixed and placed in a water bath for at least 10 minutes while stirring. Then, the container was transferred onto an ice bath for at least 60 additional minutes. At this stage, the gels turn from white and opaque to transparent and homogeneous looking liquid solution. Finally, the gel was stored for at least 12 hours at 1-4 ℃ before measurements.

2.2. Experimental setup

Before the experiments, the gel was molded into into an adjustable aluminum vessel with cross sectional area of $80\times80mm$, 8 mm wall thickness and adjustable gel thickness, with two piezoresistive sensors cemented on the faces. One mm thick aluminum sheets were placed between the gel and the sensors in order to apply initial pressure on the sensors. Reference experiments without gel were performed in order to ensure that the aluminum sheets and the cement do not interfere with the propagation of the stress wave. Four different thicknesses and three concentrations of the liquid gel were tested, 4, 7, 10, and 20 mm, and 5, 10 and 15 %Wt, respectively. The tests were performed after the gel settled in order to reach to room temperature and minimize porosity in the gel layer [3].

After the gel settled, the vessel was placed in a SHPB apparatus whose transmitted bar was removed (Hopkinson bar). By firing the 185 mm long projectile on the incident bar, a stress pulse of ca. 75 μSec was generated and propagated towards the gel through the vessel's wall contacting the gel. Upon reaching the gel, the force sensors recorded the stress wave before and after the gel layer, at a sampling frequency of 2 MHz. In all those experiments, the striker was located in the same depth in the muzzle of the gas gun, and the same air pressure was applied in order to generate similar initial stress wave in all the experiments. Due to the statistical nature of the amorphous gel

and in order to assess repeatability, each thickness was tested 25 times. Since the gelation process is completely reversible without memory effect, a virtually unlimited number of experiments can be performed on the same gel batch. All the experiments were carried at room temperature ($22 \pm 3\,^{\circ}\mathrm{C}$) in ambient air, so that the gel was in its liquid phase. The experimental setup and its components are presented in Fig. 1.

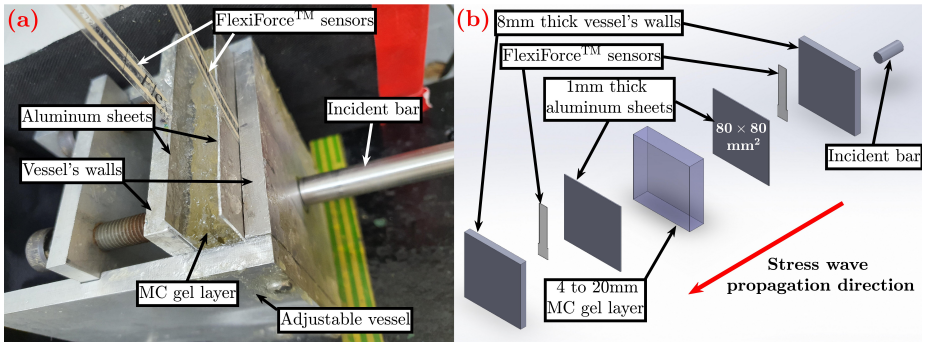

Figure 1: (a) A photograph of the experimental setup for 20mm MC gel. (b) Schematic description of the experimental setup. Note that the shock is applied on the aluminum wall contacting the gel.

2.3. Reference water experiments

Water experiment with 4 thicknesses were performed, each thickness was tested 10 times. Those observations were considered as a 0%Wt MC gel and also were used to assess the negligible geometrical attenuation of the experimental setup.

2.4. Statistical analysis

In order to reduce the statistical scatter of the experimental results, each combination of thickness and concentration (12 test groups) was tested 25 times. Chi-squared normality test was performed on each group, the null hypothesis being that the data comes from a population which distributes normally. The results were then fitted to a normal distribution function. Normal distribution fitting was carried out after excluding the outliers of each group, defined as

observations whose value exceeds three time the *Median Absolute Deviation* (MAD), defined as:

$$\text{MAD} = \text{median}\left(|A_i - \text{median}(A)|\right) \tag{1}$$

Where A_i is the i^{th} observation within group A.

Two-way *Analysis of variance* (ANOVA) test [14] was performed on the experimental results in order to examine the effect of the concentration and the thickness on the attenuation. Three F-tests [14] were performed to assess the effect of the thickness, the concentration and their potential interaction on the attenuation. For each test, the null hypothesis was that all the results were taken from the same group with certain characteristics, i.e. the change in the thickness and concentration does not affect the attenuation. For P-values smaller than 0.05, the null hypothesis is rejected and the conclusion is that the change in those parameters does indeed affect the results.

2.5. Attenuation analysis

2.5.1. Frequency decomposition

In order to examine the frequency dependent attenuation, it is necessary to estimate the *frequency response function* $H(f)$. $H(f)$ is a function which returns the attenuation of each frequency component f. An unbiased estimate for $H(f)$ can be calculated as follows [15]:

$$\tilde{H}(f) = \frac{\tilde{S}_{xy}(f)}{\tilde{S}_{xx}(f)} \tag{2}$$

Where $\tilde{H}(f)$ is the estimated frequency response function, $\tilde{S}_{xy}$ is the cross power spectral density (CPSD) of F_{in} and F_{out} (measured forces on both sides of the gel sample), and $\tilde{S}_{xx}$ is the power spectral density (PSD) of F_{in}. The CPSD and the PSD are defined as the Fourier transform of the cross-correlation and auto-correlation functions respectively. $\tilde{H}(f)$ is a discrete function that describes the attenuation of force components as a function of their frequencies.

2.5.2. Impulse attenuation

In addition to these spectral attenuation characteristics, it is necessary to examine the total physical attenuation of the material, namely impulse attenuation [16]. For this purpose, the total attenuation was calculated using the incoming and outcoming impulses. The experimental results, i.e. the signals from the FF sensor before (F_{in}) and after the gel (F_{out}) and the signal from the SG on the incident bar were recorded.

For the FF signals, the incoming and outcoming impulses were calculated according to Eq. 3.

$$J = \int_0^\tau F \, dt \tag{3}$$

Where J is the impulse, τ is the duration of the pulse and F is the measured force signal (F_{in} or F_{out}).

From the incoming J_{in} and outcoming J_{out} impulses, the attenuation factor was defined according to Eq. 4.

$$\mathrm{AF} = \frac{J_{in} - J_{out}}{J_{in}} \cdot 100\% \tag{4}$$

Note that instead of processing forces, which may contain sharp peaks and oscillations, an integral variable, such as the impulse, reduces noticeably the effect of those sharp oscillations on the calculated attenuation factor.

3. Experimental Results

3.1. Wave velocity measurement

As a first step, the longitudinal wave velocity of the gel was calculated. For each concentration, the time between the force measurements before and after the gel was calculated. The propagation time was taken as the time lag which provided the maximal cross-correlation between the incoming and outcoming signal. Then, the wave propagation velocity was calculated by dividing the thickness of the gel by the propagation time. For pure water, the average wave

velocity was found to be ca. 1400 $\left[\frac{m}{sec}\right]$ while for MC hydrogels, the wave velocity was ca. 300 $\left[\frac{m}{sec}\right]$ for 5%Wt and ca. 200 $\left[\frac{m}{sec}\right]$ for 15%Wt.

3.2. Frequency dependence of attenuation

For each test, the estimated frequency response function $\tilde{H}(f)$ was calculated according to Eq. 2. The averaged functions for each test group are presented in Fig. 2. The markers present the average value of $\tilde{H}(f)$ for each frequency and the error bars represent the standard deviation of the observation around the average value.

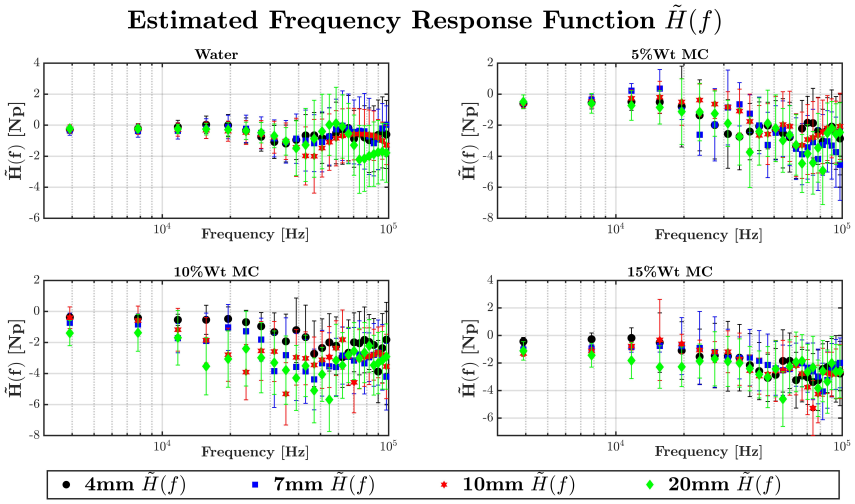

Figure 2: Estimated frequency response functions $\tilde{H}(f)$ for different thicknesses and concentrations

According to the sensors' manufacturer data, the sensors' minimal response time for impact experiments is $5 \cdot 10^{-6}$ seconds, which allows measuring frequencies up to 200 KHz. When examining the frequency content of the signals, it was found that the frequency content of a typical signal does not exceed 100 kHz. Therefore, all the frequency components exceeding 100kHz were neglected. For those high frequencies, the normalized power intensity was less than 0.05 and therefore both power spectral densities $\tilde{S}_{xx}$ and $\tilde{S}_{xy}$ are small. Those cutoff frequencies do not contain significant amount of energy and neglecting them

prevents the noises caused by the division of those 2 small quantities without affecting the experimental results significantly.

3.3. Thickness and concentration dependence of impulse attenuation

Let us now consider the effects of the gel layer's thickness and concentration. For each test, the attenuation factor (AF) was calculated as per Eq. 4. The distributions of AF for each group are presented in Fig. 3.

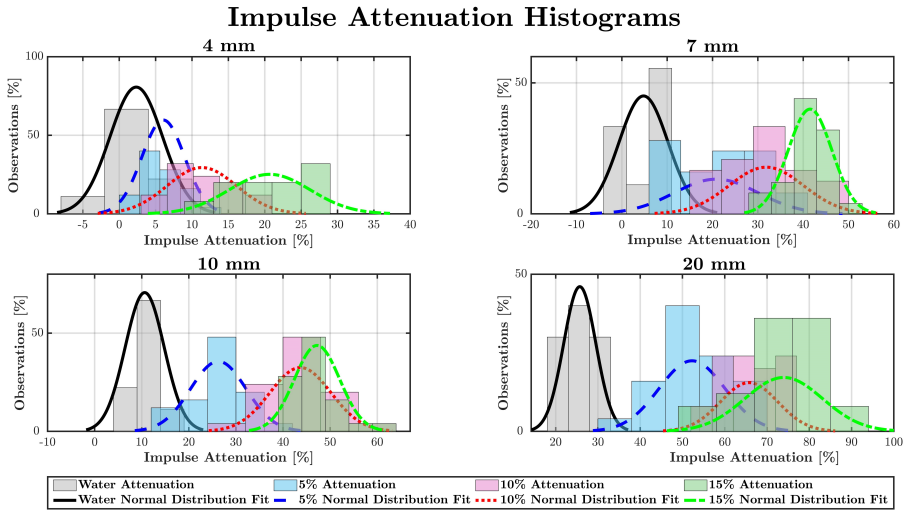

Figure 3: Experimental impulse attenuation factors distribution for different thicknesses and concentrations

Normality test was performed on each test group. The test showed normal behavior for each of the groups with significance level of 0.05. Then a normal distribution function was fitted to the experimental results. The distribution coefficients, the mean μ and the standard deviation σ are listed in Table 1.

In order to examine the effect of the concentration and the thickness on the attenuation factor, two-way ANOVA test was performed, whose results are listed in Table 2.

Note that the P-values for all factors are small, indicating a strong effect of the thickness and the concentration. In addition, there is a significant interaction between the thickness and the concentration as shown in the third

	Water				**5%Wt**			
	4mm	7mm	10mm	20mm	4mm	7mm	10mm	20mm
μ[%]	2.35	4.79	10.63	25.71	6.06	20.85	26.26	52.26
σ[%]	3.63	5.42	4.14	3.81	2.94	9.28	5.91	7.82
	10%Wt				**15%Wt**			
	4mm	7mm	10mm	20mm	4mm	7mm	10mm	20mm
μ[%]	11.36	31.87	43.69	65.77	20.69	41.52	47.22	73.95
σ[%]	4.77	8.21	6.49	6.79	5.58	4.83	4.82	9.21

Table 1: Impulse attenuation normal distribution coefficients

Source	SS	DF	MS	F test	Prob > F
Concentration	19351.2	2	9675.6	209.03	0
Thickness	101321.6	3	33773.9	729.66	0
Interaction	1079.8	6	180	3.89	0.0009
Error	13330.7	288	46.3		
Total	135083.2	299			

Table 2: Two-way ANOVA test

row. Consequently, one can now fit those attenuation results with a non-linear function, of both the concentration and the thickness, as discussed in the sequel.

4. Modeling

4.1. Frequency dependent attenuation model

The average frequency response functions for each thickness and concentration are presented in Fig. 2. For each concentration, the frequency response functions for different thicknesses overlap and show the same behavior. Therefore, as a first approximation, it is possible to neglect the effect of the thickness on the frequency attenuation. The functions for different thicknesses for each concentration were averaged, the average functions for each concentration are presented in Fig. 4.

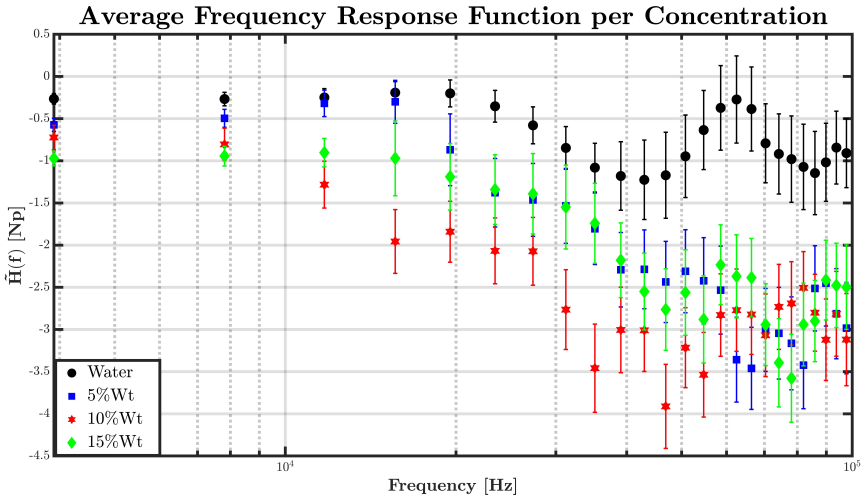

Figure 4: Estimated frequency response functions for each concentration. The functions were averaged for all thicknesses with the same concentration

The estimated frequency response functions of the gel, i.e. 5, 10 and 15%Wt, shows a similar behavior in the tested frequency domain. The attenuation of the gel grows with the frequency up to ca. 60kHz, as reported by Rotbaum et al. [8]. On the other hand, the frequency response function of the water shows a different behavior without significant growth of the attenuation with the frequency. As another approximation, the frequency response functions of the gel were averaged, and the final function is presented in Fig. 5, noting that the attenuation here is presented on linear scale.

The average function of all the thicknesses and gel concentrations shows uniform attenuation up to 10kHz, growing attenuation between 10 to 40 kHz, and then uniform attenuation between 40 to 100 kHz.

A candidate function which display a similar sigmoid trend is the *error function* $\mathrm{erf}(z)$:

$$\mathrm{erf}(z) = \frac{2}{\sqrt{\pi}} \int_0^z e^{-t^2} dt \tag{5}$$

Based on its sigmoid behavior, shifted error function was fitted to the ex-

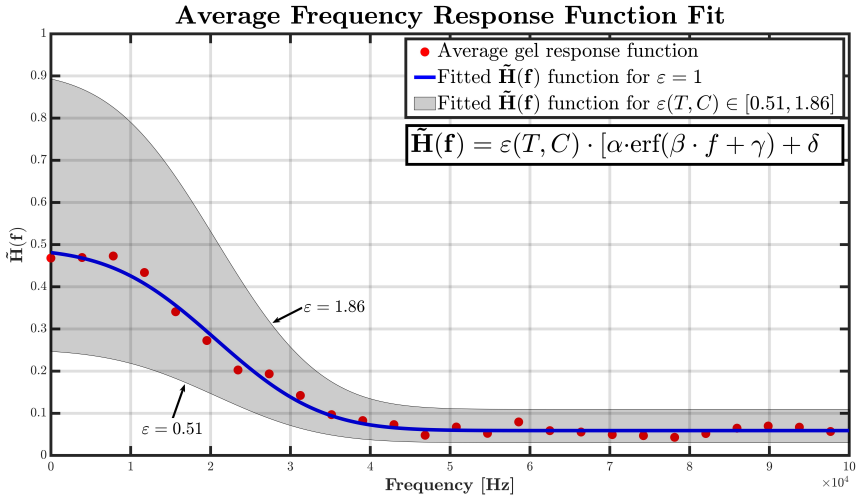

Figure 5: Fitted frequency response function. The grey area represents the function for higher and lower impulse attenuation factors as detailed in Section. 4.3. Note that $\tilde{H}(f)$ is dimensionless and not presented in [Np] like in Fig. 2 and 4

perimental results. The Fitted function is presented in Eq. 6.

$$\tilde{H}(f) = \alpha \cdot \mathrm{erf}(\beta \cdot f + \gamma) + \delta \tag{6}$$

Where $\tilde{H}(f)$ is the frequency attenuation function, f is the frequency in Hz and α, β, γ and δ are constants. The fitted function is presented in Fig. 5, the grey area around the fitted function represents a modification which will be discussed in Section 4.3, the values of α, β, γ and δ are detailed in Table. 3.

Constant	α	$\beta \left[\frac{1}{\mathrm{Hz}}\right]$	γ	δ
Value	-0.216	$6.82 \cdot 10^{-5}$	-1.411	0.275

Table 3: Frequency dependent model constants

4.2. Impulse attenuation model

As measured, the attenuation factor for a certain concentration must increase with the thickness. Therefore, the mathematical requirements on the fitted

function are a monotonic increasing function with the thickness. In addition, the attenuation with no gel layer must be zero and the attenuation cannot exceed 100% for higher thicknesses. A candidate function meeting those requirements is shown in Eq. 7.

$$AF(T) = 100 \cdot \left(1 - e^{-b \cdot T}\right) \tag{7}$$

Where AF is the expected attenuation factor, T is the thickness and b is a material constant.

This suggested function was fitted to the experimental results of each concentration. The fitted function are presented in Fig. 6. The values of the model constants b are detailed in Table 4.

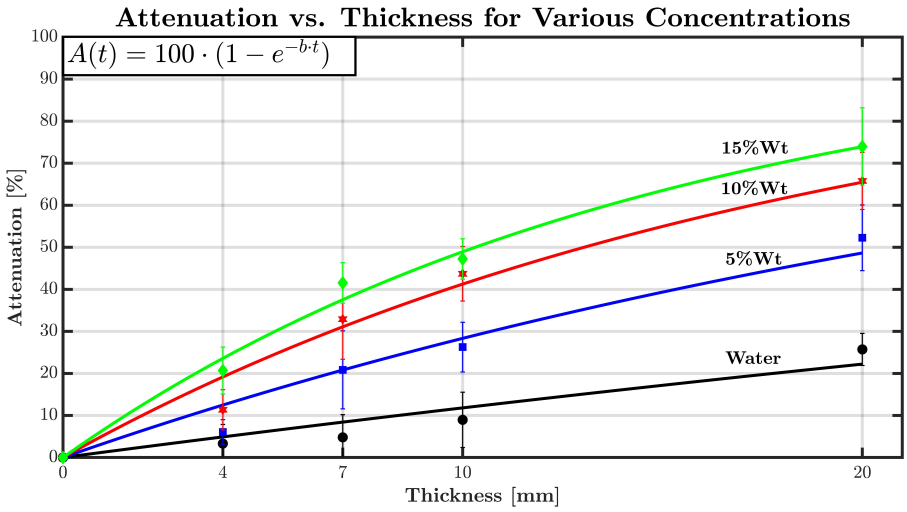

Figure 6: Attenuation-thickness relation for each concentration

	Water	5%Wt	10%Wt	15%Wt
b $\left[\frac{1}{mm}\right]$	0.01256	0.03332	0.05317	0.06721

Table 4: Model constant b for various concentrations

The fitted function is monotonically increasing with a decreasing slope at increasing thickness. Examining the connection between the constant b and the

concentration, shows positive linear relation the constant and the concentration. That can be fitted with a 1st order polynomial

After suggesting a relation between the attenuation and the thickness, and finding a linear relation between the constant b and the concentration, it is possible to obtain a full model by replacing the constant b with a linear function of the concentration. The following relation between the attenuation factor, the thickness and the concentration is obtained.

$$AF(T, C) = 100 \cdot \left[1 - e^{-(a \cdot C + b) \cdot T}\right] \tag{8}$$

Where AF is the expected attenuation factor (%), T is the thickness (mm), C is the concentration (%Wt), and a and b are material constants (see units in Table 5). The fitted function is presented in Fig. 7, the constants detailed in Table 5. The data point and the black lines present the mean μ and the standard deviation σ for each test group as detailed in Table 1.

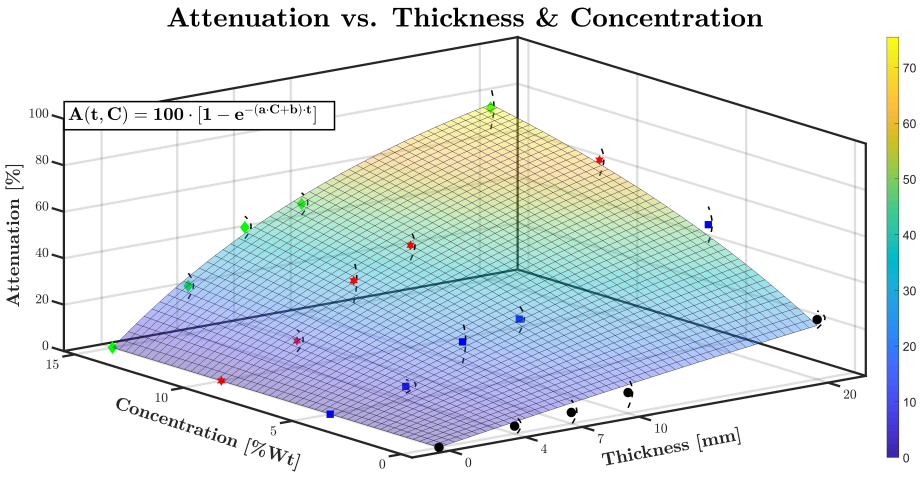

Figure 7: Impulse attenuation as a function of both gel thickness and the concentration

4.3. Combining spectral and impulse attenuation into one model

The spectral attenuation model, which detailed in Eq.6, describes the shape of the attenuated signal but not necessarily its amplitude. This amplitude is

Constant	$a\left[\frac{1}{\%Wt \cdot mm}\right]$	$b\left[\frac{1}{mm}\right]$
Value	0.0038	0.0131

Table 5: Experimental material constants

represented by the impulse attenuation function in Eq.8. However, the latter is an integral attenuation equation, providing an average figure for the whole signal and not for its spectral components.

In order to match the impulse and the frequency attenuation models, we suggest the following modification. Assume the frequency attenuation function is now multiplied by $\varepsilon(T, C)$ where $\varepsilon(T, C)$ is thickness and concentration dependent. This modification, for $\varepsilon(T, C) \in [0.51, 1.86]$, which are the minimal and maximal values which were obtained from the experimental signals, is marked as grey area around the fitted function in Fig. 6. The determination of $\varepsilon(T, C)$ is detailed in the sequel.

Assume an incoming signal F_{in} for thickness T and concentration C. The frequency decomposition of F_{in} can be calculated using Fourier transform:

$$\tilde{f}_{in}(f) = \mathcal{F}[F_{in}(t)] \tag{9}$$

Where $F_{in}(t)$ is the incoming signal in the time domain and $\tilde{f_{in}}(f)$ is the transformed signal in the frequency domain, the symbol $\mathcal{F}$ representing the Fourier transform.

The spectrum of the pulse after the gel layer can be calculated according to Eq. 6:

$$\tilde{f}_{out}(f) = \varepsilon(T, C) \cdot \tilde{H}(f) \cdot \tilde{f}_{in}(f) \tag{10}$$

The outcoming pulse in the time domain can be calculated by inverse Fourier transform. Due to the linearity of Fourier transform, the coefficient $\varepsilon(T, C)$ can be extracted from the inverse transform:

$$F_{out}(t) = \mathcal{F}^{-1}[\tilde{f}_{out}(f)] = \varepsilon(T, C) \cdot \mathcal{F}^{-1}[\tilde{H}(f) \cdot \tilde{f}_{in}(f)] \tag{11}$$

Denote the impulse of the outcoming pulse before the modification ($\varepsilon(T,C) = 1$) as J^*_{out}:

$$J^*_{out} = \int_0^\tau \mathcal{F}^{-1}[\tilde{H}(f) \cdot \tilde{f}_{in}(f)]\, dt \tag{12}$$

The coefficient $\varepsilon(T,C)$ is required to set the impulse of the outcoming pulse according to Eq. 8. Since $\varepsilon(T,C)$ is time independent, the final outcoming impulse J_{out} is:

$$J_{out} = \varepsilon(T,C) \cdot J^*_{out} \tag{13}$$

The impulse attenuation factor should fit to the model detailed in Eq. 8,namely:

$$\mathrm{AF}(T,C) = \frac{J_{in} - J_{out}}{J_{in}} \cdot 100\% = \frac{J_{in} - \varepsilon(T,C) \cdot J^*_{out}}{J_{in}} \cdot 100\% \tag{14}$$

Therefore, the value of $\varepsilon(T,C)$ is:

$$\varepsilon(T,C) = \left(1 - \frac{\mathrm{AF}(T,C)}{100}\right) \cdot \frac{J_{in}}{J^*_{out}} \tag{15}$$

Where $\mathrm{AF}(T,C)$ is the predicted impulse attenuation factor according to Eq. 8, J_{in} is the impulse of the incoming pulse and J^*_{out} is the impulse of the outcoming pulse before the modification according to Eq. 12, namely $\varepsilon(T,C) = 1$.

This process can both predict the shape and the impulse of the outcoming pulse for a given gel thickness, concentration and incoming pulse. First, the shape of the outcoming pulse is determined according to the incoming spectrum and the frequency response function $\tilde{H}(f)$. Then, the outcoming pulse is multiplied by a correction coefficient $\varepsilon(T,C)$ in order to set the correct impulse attenuation according to Eq. 8.

4.4. Model validation

In this part, the suggested model was tested on real experimental signals. Typical incoming signals that were recorded from tests on 5, 10 and 15%Wt gel

layers of various thicknesses were processed according to the suggested model. First, the signals were decomposed into their frequency content. Next, each frequency of each spectrum was multiplied by its suitable attenuation according to Eq.6. Finally, the outcoming signals were re-composed and multiplied by the calculated $\varepsilon(T, C)$, in order to determine the real impulse attenuation Eq.8.

To illustrate this point, consider the 10%Wt-4mm case shown in Fig.8. An incoming signal with impulse of $J_{in} = 0.0548[N \cdot Sec]$ was processed according to Eq. 6. Then, the signal was re-composed and its impulse J^*_{out} was found to be $0.0263[N \cdot Sec]$. According to Eq. 8, the impulse attenuation factor for 10%Wt and 4mm gel should be 18.48% and therefore the outcoming pulse is multiplied by the coefficient $\varepsilon(4, 10) = 1.6956$ which is calculated according to Eq. 15, in order to set the suitable impulse attenuation factor.

Three examples of signals from all 3 tested concentrations are presented in Fig. 8. The simulated signals are compared to the real outcoming signals which were measured in the experiments. It should be noted that the simulated signals were calculated according to an average model. Here, the averaging process is equivalent to a low pass filter, therefore the simulated attenuated outcoming-signals are a filtered version of the of the measured ones. Despite this limitation, the matching between experimental and predicted attenuated signals is excellent.

5. Discussion

This research brings further systematic information of the shock attenuation characteristics of thermo-reversible MC gels. Three specific parameters are considered, namely frequency content of the shock, gel concentration and gel thickness.

In this work, we consider pure water both as a reference fluid, in order to distinguish between the gel attenuation and the eventual geometric dissipation due to the experimental setup, but also as the 0%wt reference. All the parameters of the gel, whether momentum attenuation or frequency analysis clearly

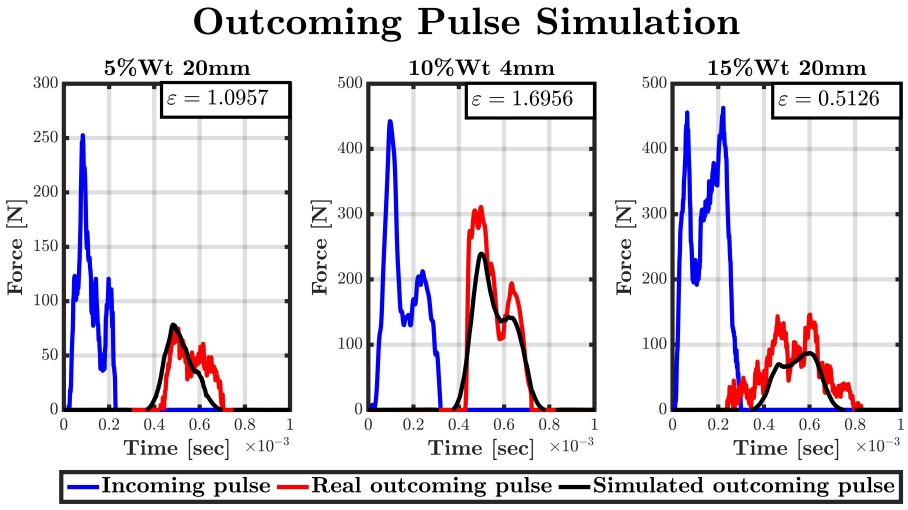

Figure 8: Comparison between measured and simulated outcoming signals

show that a minute concentration of MC, 5%wt, is sufficient to differentiate the gel from water to a significant extent.

Impulse attenuation is considered as more representative than force attenuation for its integral character. The impulse attenuation factor for any test group is found to be near normally distributed, increasing with the gel thickness and concentration. A simple expression was fitted for all the investigated gel thicknesses and compositions.

While the impulse attenuation represents a global attenuation capacity of the MC gel, somewhat like a "black box", additional precious information is gained by examining this property on a spectral basis. The first important outcome is that MC gels attenuate the various frequency components in the range of frequencies of up to 100 kHz. It is important to note that this range of frequencies is definitely relevant to structural shocks, which renders those gels particularly attractive and effective. One can also observe that the spectral attenuation is independent of the gel thickness and composition, to a first approximation. This indicates that frequency attenuation is a pure material property of the gel, irrespective of its composition or geometry.

It is interesting to note that for a typical phase velocity of the order of 300 $\left[\frac{m}{sec}\right]$, the wavelength of a 5 kHz signal is 60 mm, reducing to 3 mm at 100 kHz. We observe a lesser attenuation of frequencies below 40 kHz, corresponding to a 7.5 mm wavelength, that is of the order of the investigated gel thickness. While all frequencies are attenuated to some extent, it appears that those, for which the wavelength is smaller than the gel's thickness are significantly more attenuated than those whose wavelength is of the order of the gel thickness.

The interesting outcome of those two types of attenuation is that they can be decoupled and recombined up to a coefficient $\varepsilon(T, C)$, so that geometry and composition play a role in momentum attenuation while frequency attenuation determines essentially the shape of the attenuated signal.

The material model for impulse attenuation of MC gels was validated by replicating 3 independent experimental sets of pulses. The results presented in this work can be incorporated into numerical simulations of protective systems, with emphasis on bodily traumatic injuries.

6. Conclusions

- The impulse attenuation of the gel is strongly affected by the gel's concentration and thickness, with a strong interaction between these parameters.
- This attenuation is frequency dependent in the structural range of frequencies smaller than 100 kHz, irrespective of the gel composition or thickness in the range of investigated parameters of this study.
- The shock attenuation of MC hydrogels has been modelled in a way that allows incorporation into numerical simulations of protective systems, among which those aimed at reducing traumatic organ injury.

Declaration of Competing Interest

The authors declare that they have no known competing financial interests or personal relationships that could have appeared to influence the work reported in this paper.

Acknowledgements

This research was partly supported by grant 2024374 from the Technion PMRI Center for Security Science and Technology.

The authors wish to acknowledge Prof. Y. Eichen and Dr. G. Parvari, Schulich Faculty of Chemistry – Technion, for many enlightening discussions and assistance with the preparation of the gel samples.

References

[1] N. Schupper, N. M. Shnerb, Inverse Melting and Inverse Freezing: A Spin Model, Physical Review E - Statistical, Nonlinear, and Soft Matter Physics 72 (10) (2005) 1–16. doi:10.1103/PhysRevE.72.046107.

[2] G. Parvari, Y. Rotbaum, Y. Eichen, D. Rittel, Impact-induced Gelation in Aqueous Methylcellulose Solutions, Chemical Communications 54 (9) (2018) 12578–12581. doi:10.1039/c8cc06378h.

[3] K. Senol, G. Parvari, Y. Rotbaum, Y. Eichen, D. Rittel, A. Shukla, Mitigation of Shock Loading on Structures using Aqueous Methylcellulose Solution, International Journal of Impact Engineering 140 (2) (2020) 734–743. doi:10.1016/j.ijimpeng.2020.103547.

[4] M. D. Alley, B. R. Schimizze, S. F. Son, Experimental Modeling of Explosive Blast-related Traumatic Brain Injuries, NeuroImage 54 (5) (2011) S45–S54. doi:10.1016/j.neuroimage.2010.05.030.

[5] L. Cui, S. Kiernan, M. D. Gilchrist, Designing the Energy Absorption Capacity of Functionally Graded Foam Materials, Materials Science and Engineering A 507 (12) (2009) 215–225. doi:10.1016/j.msea.2008.12.011.

[6] Z. Noemi, Edible Coatings to Improve Food Quality and Safety, in: Food Engineering Interfaces, Springer, 2011, pp. 631–660. doi:10.1007/978-1-4419-7475-4_27.

[7] Y. Rotbaum, G. Parvari, Y. Eichen, D. Rittel, Mechanical Reinforcement of Methylcellulose Hydrogels by Rigid Particle Additives, Mechanics of Materials 132 (2) (2019) 57–65. doi:10.1016/j.mechmat.2019.02.013.

[8] Y. Rotbaum, G. Parvari, Y. Eichen, D. Rittel, Linear and Nonlinear Shock Attenuation of Aqueous Methylcellulose Solutions, International Journal of Impact Engineering 136 (9) (2019) 103392. doi:10.1016/j.ijimpeng.2019.103392.

[9] H. Kolsky, An Investigation of the Mechanical Properties of Materials at Very High Rates of Loading, Proceedings of the Physical Society. Section B 62 (10) (1949) 676–700. doi:10.1088/0370-1301/62/11/302.

[10] W. Chen, B. Song, Split Hopkinson (Kolsky) Bar Design, Testing and Applications, Springer, 2011. doi:10.1007/978-1-4419-7982-7.

[11] W. Chen, B. Zhang, M. J. Forrestal, A Split Hopkinson Bar Technique for Low-impedance Materials, Experimental Mechanics 39 (10) (1998) 81–85. doi:10.1007/BF02331109.

[12] J. Kwon, G. Subhash, Compressive Strain Rate Sensitivity of Ballistic Gelatin, Journal of Biomechanics 43 (10) (2010) 420–425. doi:10.1016/j.jbiomech.2009.10.008.

[13] D. Richler, D. Rittel, On the Testing of the Dynamic Mechanical Properties of Soft Gelatins, Experimental Mechanics 54 (1) (2014) 805–815. doi:10.1007/s11340-014-9848-4.

[14] H. Sahai, M. M. Ojeda, Analysis of Variance for Random Models, Vol. 2, Birkhäsuser, 2005. doi:10.1007/b138864.

[15] K. Shin, J. Hammond, Fundamentals of Signal Processing for Sound and Vibration Engineers, Wiley, 1996.

[16] T. Rahimzadeh, E. M. Arruda, M. D. Thouless, Design of Armor for Protection against Blast and Impact, Journal of the Mechanics and Physics of Solids 85 (9) (2015) 98–111. doi:10.1016/j.jmps.2015.09.009.